

## Consequences of zero-point motion to the radial distribution function of amorphous silicon

This content has been downloaded from IOPscience. Please scroll down to see the full text.

2004 J. Phys.: Condens. Matter 16 S5165

(<http://iopscience.iop.org/0953-8984/16/44/013>)

View [the table of contents for this issue](#), or go to the [journal homepage](#) for more

### Download details:

IP Address: 129.174.252.90

This content was downloaded on 06/10/2016 at 18:02

Please note that [terms and conditions apply](#).

You may also be interested in:

[Binary continuous random networks](#)

Normand Mousseau and G T Barkema

[The inclusion of experimental information in first principles modelling of materials](#)

Parthapratim Biswas, De Nyago Tafen, Raymond Atta-Fynn et al.

[Crystallization study of model tetrahedral semiconductors](#)

S M Nakhmanson and N Mousseau

[Dominant structural defects in amorphous silicon](#)

Paule Dagenais, Laurent J Lewis and Sjoerd Roorda

[Real space information from fluctuation electron microscopy: applications to amorphoussilicon](#)

Parthapratim Biswas, Raymond Atta-Fynn, S Chakraborty et al.

[Quantum atomic dynamics in amorphous silicon; a path-integral Monte Carlo simulation](#)

Carlos P Herrero

[Understanding subtle changes in medium-range order in amorphous silicon](#)

Paule Dagenais, Laurent J Lewis and Sjoerd Roorda

## Consequences of zero-point motion to the radial distribution function of amorphous silicon

Joseph L Feldman<sup>1</sup>, Noam Bernstein, Dimitris A Papaconstantopoulos and Michael J Mehl

Center for Computational Materials Science, Naval Research Laboratory, Washington, DC 20375, USA

E-mail: feldman@dave.nrl.navy.mil

Received 8 September 2004

Published 22 October 2004

Online at [stacks.iop.org/JPhysCM/16/S5165](http://stacks.iop.org/JPhysCM/16/S5165)

doi:10.1088/0953-8984/16/44/013

### Abstract

While there have been many studies based on models of amorphous silicon, there have been surprisingly few (perhaps only one) that have seriously addressed the radial distribution function at low temperature. Our work is based in part on the so-called NRL tight binding method using parameters for silicon determined by Bernstein *et al.* As we have recently shown in the case of 216-atom models, upon including zero-point motion good agreement is obtained with very accurate low temperature x-ray diffraction measurements by Laaziri *et al* of the radial distribution function, although, as also found by Herrero who used the Stillinger–Weber potential, a slight asymmetry of the first peak in the RDF is predicted and this asymmetry has not been observed experimentally. Upon use of an estimate of zero-point broadening from our previous work we show here that 1000-atom models lead to good agreement with experiment for the RDF. Perhaps fortuitously, we obtain models that agree with the experimentally determined second peak in the RDF for both annealed and unannealed samples: our tight binding relaxed models based on topologies derived from the Wooten–Winer–Weaire method and the Barkema–Mousseau method yield unannealed-sample results, whereas our tight binding relaxed model based on an MD quench of the liquid using the semi-empirical interatomic potential, EDIP, of Kaxiras and coworkers yield the annealed-sample results. Finally, the significant effect of zero-point motion on the first peak in the radial distribution that we obtain in the case of amorphous silicon could also have implications for other amorphous materials, e.g. SiO<sub>2</sub>.

<sup>1</sup> Author to whom any correspondence should be addressed.

## 1. Introduction

The natural breadth of the first peak in the radial distribution function (FPRDF) of amorphous silicon was only recently observed for the first time by Laaziri *et al* [1] by carrying out x-ray diffraction measurements out to a sufficiently large  $Q_{\max}$  (maximum value of the magnitude of the diffraction vector). Their results from a polycrystal at  $T = 10$  K suggest that even at this temperature the FPRDF of amorphous silicon is substantially broadened beyond the inherent static structural broadening. They obtained data for as-implanted and annealed samples and concluded that the average coordination is approximately 3.88 for the former and 3.79 for the latter. We have previously applied [2] the NRL tight-binding (TB) method to simulations of vibrational, elastic, and structural properties of two 216-atom models. We found that conclusions by Laaziri *et al* for the coordination might be modified if one allowed for asymmetry in the FPRDF, an asymmetry that we observed computationally both before and after applying zero-point broadening, although it is substantially more apparent in the former case. Here we present in more detail the zero-point broadening parameter computed for one of our 216-atom models, and apply it approximately to larger models. We study 1000-atom models generated by several methods:

- (a) the Wooten–Winer–Weaire (W) bond switching algorithm [3];
- (b) quenching of the liquid state via molecular dynamics and the environment-dependent interatomic potential (EDIP) [4];
- (c) an improved Wooten–Winer–Weaire method, Barkema and Mousseau (BM) [5];
- (d) relaxation of W, EDIP, and BM models using the conjugate gradient method with forces computed with the NRL-TB approach (the relaxed models are denoted by TB-W, TB-EDIP, and TB-BM, respectively).

Compared to our original work this new analysis gives better statistics, allows us to examine the RDF at longer distances, and adds a structural model generated with another method.

## 2. Brief discussion of NRL tight binding

In this scheme tight binding parameters are represented by polynomial functions of interatomic distances fitted to the total energy and eigenvalues of first-principles LAPW/LDA calculations [6]. The tight binding Hamiltonian representational basis is non-orthogonal and the sum of eigenvalues of the occupied states gives the total energy. For silicon we use the  $sp^3$  basis and include in the fit the *crystalline* diamond-, FCC-, BCC- and SC-structure total energies (versus volume) and electron band energies [7].

## 3. Brief discussion of theory for RDF

The expression for the measured RDF is

$$J(r) = (1/N) \left\langle \sum_{i \neq j} \delta(r - r_{ij}) \right\rangle, \quad (1)$$

where the brackets denote the statistical mechanical average. To our knowledge, prior to our work only Herrero [8] calculated this quantity for an amorphous system within a quantum mechanical framework as he performed path-integral Monte Carlo calculations for  $J(r)$  with use of the Stillinger–Weber potential [9]. That procedure takes into account possible large

displacements from equilibrium. However, the small displacement, harmonic approximation ought to be sufficiently accurate at low temperature. In this latter approximation,

$$J(r) = \frac{1}{N} \sum_{i \neq j} \frac{1}{\sqrt{2\pi U_{ij}^r}} \exp(-(r_{ij}^0 - r)^2 / (2U_{ij}^r)), \quad (2)$$

where

$$U_{ij}^r \equiv \langle (\hat{\mathbf{r}}_{ij}^0 \cdot \mathbf{u}_{ij})^2 \rangle = \frac{\hbar}{8m} \sum_{\alpha} (\mathbf{e}_{ij}^{\alpha} \cdot \hat{\mathbf{r}}_{ij}^0)^2 (n + 1/2) / \omega_{\alpha}. \quad (3)$$

Here  $r$  is the distance between atoms,  $\mathbf{u}$  is an atomic displacement from equilibrium,  $\omega_{\alpha}(\mathbf{e}^{\alpha})$  is the  $\alpha$ th normal mode angular frequency (eigenvector),  $n$  is the phonon occupation number, and the subscripts indicate differences between atoms  $i$  and  $j$ . We shall also consider the so-called *static* structure factor obtained by replacing  $r_{ij}$  in equation (1) by  $r_{ij}^0$ .

#### 4. 216-atom model results for $U_{ij}^r$

In figure 1 we plot, as a function of  $r_{ij}$ , both  $U_{ij}^r$  and the bond stretching force constant (FC) discussed in [2] and shown there only over the region of the FPRDF. As shown in the bottom right panel of the figure, the nature of the bond-stretching FCs appears to bifurcate at the upper end of the second peak in the RDF and this effect is present in  $U_{ij}^r$  as well. At the upper edge of the second peak pairs of atoms of both second and third neighbours exist (note the well known absence of a peak corresponding to the third-neighbour peak in the crystal). We believe these results show the distinction in character of bonding between second- and third-neighbour interactions. The fitted curve is given by the following expression (in the units of the figure):

$$U_{ij}^r = 0.002\,616 + 0.003\,965(r_{ij} - 2.35) + 0.007\,13(r_{ij} - 2.35)^2.$$

## 5. Results

### 5.1. Energetics and structural parameters

In table 1 we give some structural parameters of interest for our TB relaxed 1000-atom models. Consistent with experiment, the density of these models at zero pressure (defined as the trace of the stress tensor<sup>2</sup>) are found to be less than the corresponding crystalline density, 0.05007 atoms  $\text{\AA}^{-3}$ . These results are given in the table in terms of the volume difference  $\delta V \equiv V_a - V_c$ . Upon inspecting the RDF we chose the value 2.8  $\text{\AA}$  as the interatomic distance below which atoms are considered to be bonded. This choice, for TB-W, yields six fivefold coordination defects, whereas, for the pristine W-model, it yields no coordination defects. In the case of TB-EDIP, there are ten threefold and 32 fivefold atoms and in the case of TB-BM there are no coordination defects. (In the table, the average coordination is denoted  $N_c$ .) Also given in the table are numbers of four-membered rings,  $N_4$ , in order to provide some indication of differences in topology among the models. The values of bond angles,  $\theta$ , are restricted to atoms which are fourfold coordinated and the values in parentheses are results of Gaussian fits to the distribution functions for values of  $\theta$ . As seen in table 1, among our three models, TB-EDIP yields the narrowest width of the distribution of bond angle deviations, although TB-BM yields the smallest RMS bond angle deviation, defined with respect to  $\theta_{\text{ave}}$ , the bond angle average. These latter values are also consistent with estimates from experiment based

<sup>2</sup> Stress tensor components of about 0.8 GPa or less are obtained due to the finite size of the models and cubic boundary conditions.

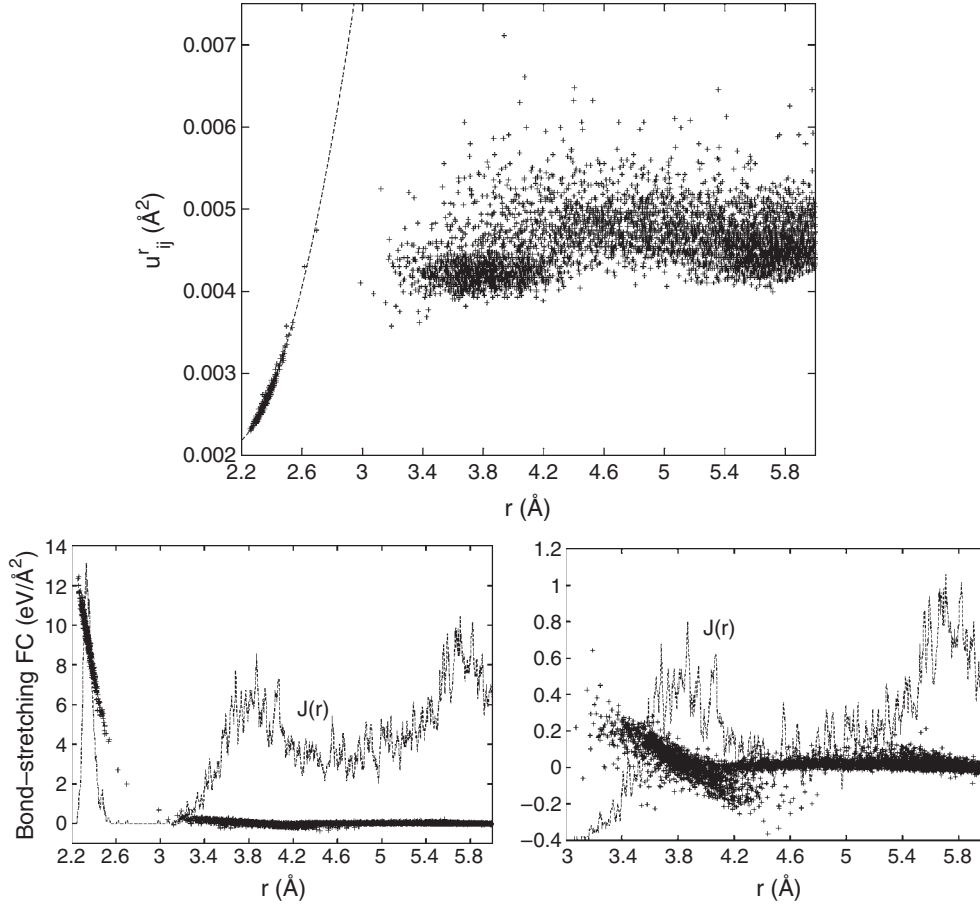


**Figure 1.** Comparison of zero-point broadening parameter, top panel, bond stretching force constant and radial dependence of the RDF, bottom two panels. The dashed curve is fitted to  $U_{ij}^r$  for  $r \leq 2.8 \text{\AA}$  (see text). The results are based on the 216-atom TB-W model.

**Table 1.** Structural parameters.

Model	$N_C$	$(\delta V)/V_c$ (%)	$N_4$	$\theta_{\text{ave}}$ (deg)	$\Delta\theta_{\text{RMS}}$ (deg)
TB-W	4.01	1.45	25	109.2 (108.8)	11.0 (10.8)
TB-EDIP	4.05	0.5	38	109.2 (108.7)	10.5(9.8)
TB-BM	4.0	1.31	0	109.2 (108.7)	10.1(10.4)
Exp.	$\leq 3.88$	$\geq 1.7$			

on the formulation of Beeman, Tsu and Thorpe [10] for the width of the ‘optic mode’ Raman peak.

Weaire [11] and Weaire and Thorpe [12] showed, with the use of a simple tight binding model, that a bandgap is obtainable even if the structure lacks crystalline periodicity. Their seminal work is strictly relevant to systems with purely topological disorder. Of course, for more realistic tight binding/structural models, even those for which all atoms are fourfold coordinated, having a clean gap is not guaranteed due to the allowed complexity of tight binding parameters and their dependences on interatomic distances. We give the electronic

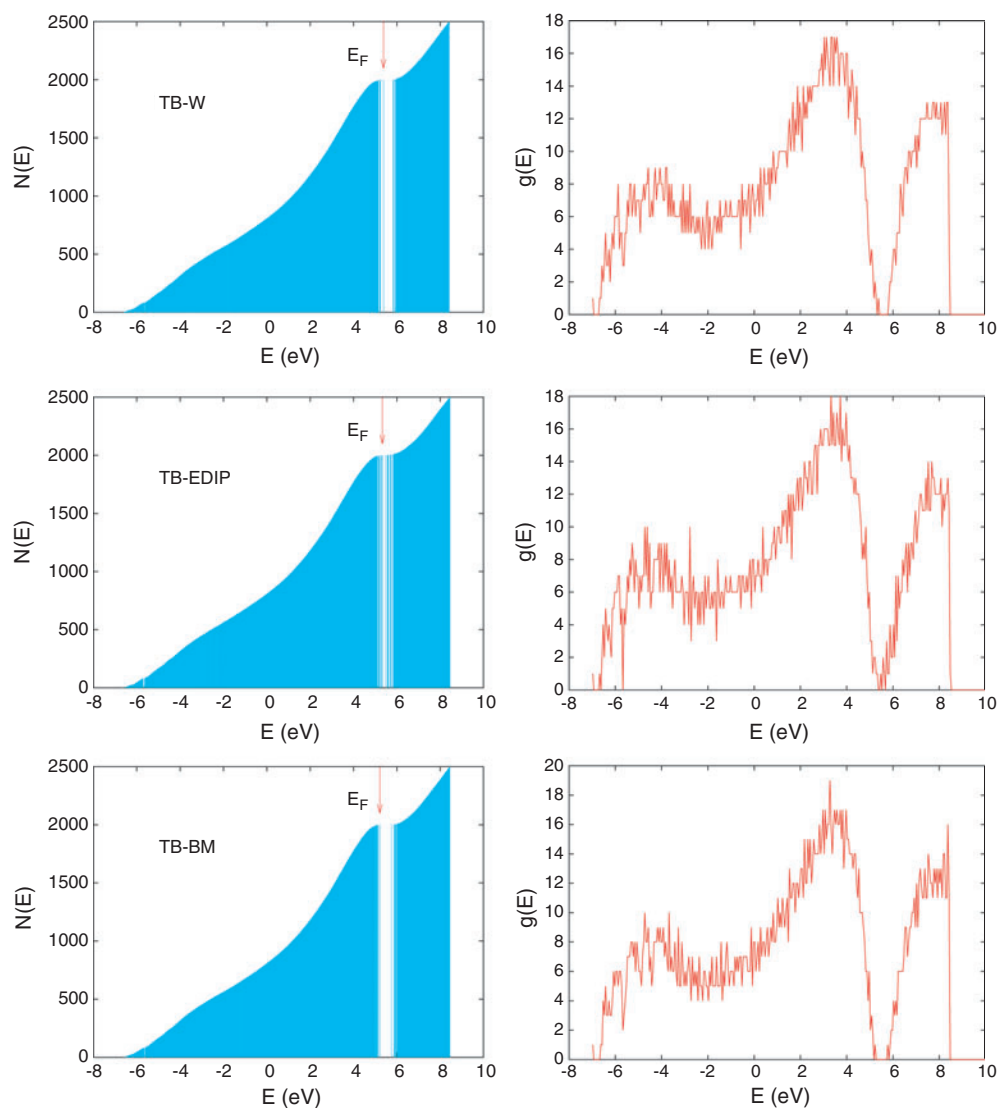


**Figure 2.** Electronic band states. Left hand figures give the integrated density of states and corresponding right hand figures give the density of states. The energy of the highest occupied state, denoted by  $E_F$ , and the total energy decrease in order for models TB-W, TB-EDIP and TB-BM.

(This figure is in colour only in the electronic version)

density of state information for the three models under consideration in figure 2. We note that our value for the gap, which is well defined only for models TB-W and TB-BM, is approximately 0.5 eV compared to the more accurate value of approximately 1 eV on the basis of *ab initio* calculations and other structural models [5, 13]. Our too small gaps are consistent with the corresponding results for the crystal; they are due to the fact that the  $sp^3$  set of tight binding parameters was not closely fitted to the LAPW/LDA results for the conduction bands of the crystal [7]. Finally, we have obtained the following results for total energies: relative to

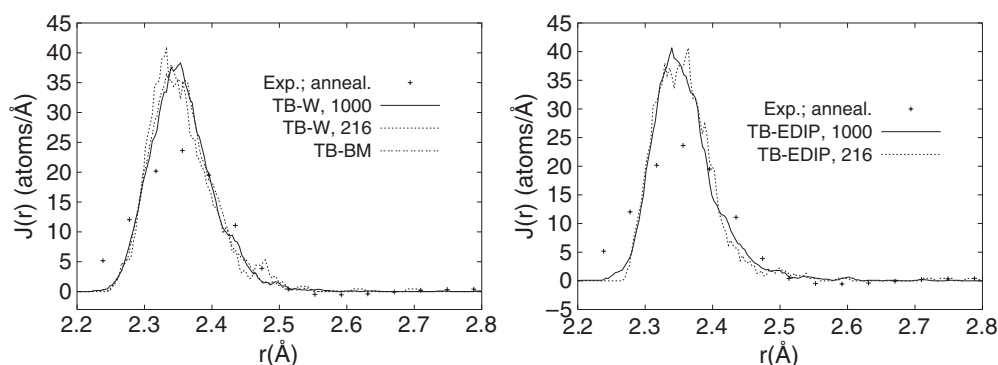


**Figure 3.** Static RDFs. Experimental data are included for comparison.

the total energy for the corresponding 1000-atom *crystalline* model at its equilibrium volume, we obtain increases of 0.2225, 0.2183, and 0.1958 eV/atom for TB-W, TB-EDIP, and TB-BM, respectively. These values are also in reasonable agreement with the quoted [4] experimental value of <0.19 eV/atom.

### 5.2. Static structural quantities

In figure 3 we give the FPRDF for TB-relaxed static structures. We see that there is reasonable agreement between the theoretical results for the 1000- and the previously obtained 216-atom models as well as among results for the three different methods of deriving the ‘pristine’ models which we relaxed. The calculated FPRDF is considerably sharper and more asymmetrical than experiment, also shown in the figure.

## 6. Zero-point broadened radial distribution function

For  $r \leq 2.8$  Å the broadening parameter,  $U_{ij}^r$  was approximated by the fitted quadratic given above and for  $r > 2.8$  Å, it was approximated by the constant value  $0.00478$  Å<sup>2</sup>. A test of this approximation in the case of 216-atom models yields negligible differences from the exact results. Finally in figures 4 and 5 we show the zero-point broadened results. There is only a small explicit zero-point effect in the region beyond the FPRDF<sup>3</sup>, because of the already-broad features in the RDF, but the zero-point broadening in the FPRDF is large as can be seen by comparing figures 3 and 4.

## 7. Conclusions

The zero-point effect in the first peak of the RDF has been shown to be important in interpreting models of amorphous silicon. As we have first discussed in another paper on 216-atom models, it has a large effect on the FPRDF within our TB approach. This result is also consistent with the interpretation of Laaziri *et al* of their experimental results on both a-Si and polycrystalline Si at low temperature. By extending our method to 1000-atom models we obtain a comparison with experiment over a larger range of distances than before, and we obtain better statistical

<sup>3</sup> Effectively, the zero-point broadening of the second peak in the RDF was discussed, on the basis of x-ray diffraction data on polycrystalline silicon, in the second reference of [1].

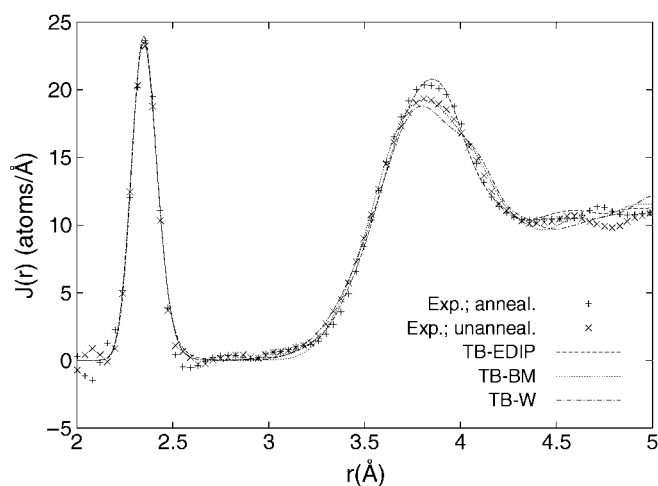


**Figure 4.** Comparison between theory and experiment [1] (at  $T = 10$  K) for first two peaks of the RDF. The theoretical quantities include the zero-point broadening (see text).

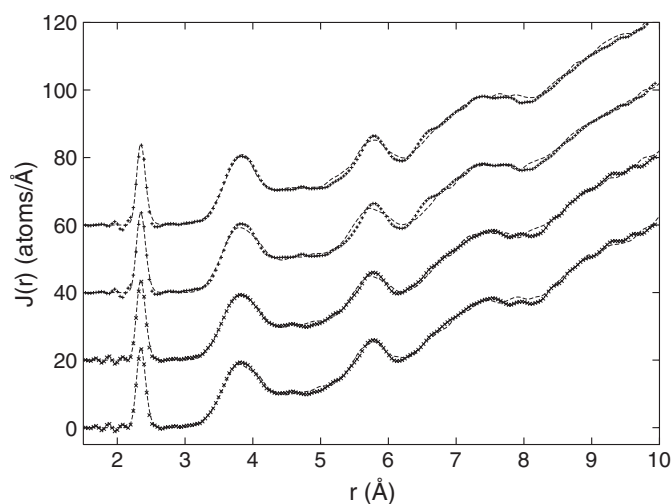


**Figure 5.** Comparison with experiment of zero-point broadened RDFs. The experimental data [1] represented in the top (bottom) two curves are for the annealed (unannealed) sample. The models represented are in the order TB-EDIP, TB-BM, TB-BM, and TB-W from top to bottom.

results at all distances. With regard to the overall RDF, we obtain tight binding relaxed models that agree well, if not exactly, with experiment for both as-implanted and annealed samples. However, the lowest energy model is the relaxed BM model which agrees best with experiment for the as-implanted sample. Perhaps, on the basis of NRL-TB, the topology of the EDIP model is superior to that of the BM model since EDIP yields good agreement for the annealed sample. However, the coordination ‘defects’ within the EDIP model represent a possibly serious deficiency of the model since the model yields numerous electronic states destroying the bandgap. Finally, the aforementioned results are based in part on a fitting procedure of the variance in the atomic displacements appropriate to zero-point broadening, for we have not yet obtained the full dynamical matrix for any of our 1000-atom models.

## Acknowledgments

This work was supported by the US Office of Naval Research. We are also grateful to Dr S Roorda for a helpful communication and for sending us the x-ray data of Laaziri *et al* [1] for the radial distribution function.

## References

- [1] Laaziri K, Kycia S, Roorda S, Chicoine M, Robertson J L, Wang J and Moss S C 1999 *Phys. Rev. Lett.* **82** 3460  
Laaziri K, Kycia S, Roorda S, Chicoine M, Robertson J L, Wang J and Moss S C 1999 *Phys. Rev. B* **60** 13520
- [2] Feldman J L, Bernstein N, Papaconstantopoulos D A and Mehl M J 2004 *Phys. Rev. B* at press  
Feldman J L, Bernstein N, Papaconstantopoulos D A and Mehl M J 2004 unpublished *Preprint* cond-mat/0405327
- [3] Wooten F, Winer K and Weaire D 1985 *Phys. Rev. Lett.* **54** 1392  
Feldman J L, Kluge M D, Allen P B and Wooten F 1993 *Phys. Rev. B* **48** 12589
- [4] Koblinski P, Bazant M Z, Dash R K and Treacy M M 2002 *Phys. Rev. B* **66** 064104
- [5] Barkema G T and Mousseau N 2000 *Phys. Rev. B* **62** 4985
- [6] Cohen R E, Mehl M J and Papaconstantopoulos D A 1994 *Phys. Rev. B* **50** 14694  
Mehl M J and Papaconstantopoulos D A 1996 *Phys. Rev. B* **54** 4519
- [7] Bernstein N, Mehl M J, Papaconstantopoulos D A, Papanicolaou N I, Bazant M Z and Kaxiras E 2000 *Phys. Rev. B* **62** 4477  
Bernstein N, Mehl M J, Papaconstantopoulos D A, Papanicolaou N I, Bazant M Z and Kaxiras E 2002 *Phys. Rev. B* **65** 249902 (erratum)
- [8] Herrero C P 1998 *Europhys. Lett.* **44** 734
- [9] Stillinger F H and Weber T A 1985 *Phys. Rev. B* **31** 5262
- [10] Beeman D, Tsu T and Thorpe M F 1985 *Phys. Rev. B* **32** 874
- [11] Weaire D 1971 *Phys. Rev. Lett.* **26** 1541
- [12] Weaire D and Thorpe M F 1971 *Phys. Rev. B* **4** 2508
- [13] Nakhmanson S M, Mousseau N, Barkema G T, Voyles P M and Drabold D A 2001 *Int. J. Mod. Phys. B* **15** 3253